CASE STUDY – Material models for depiction of unloading in low speed crash applications

B. Hirschmann[1], H. Pothukuchi[1], M. Schwab[1], Y. Nakagawa[2], N. Matsuura[2]

[1]4a engineering GmbH, Traboch, Austria
[2]Honda Motor Co., Ltd., Tochigi, Japan

1 Background and Motivation

Computer simulation is used in many fields of automobile development to shorten the development term and reduce tests. Large plastic parts such as instrument panels and bumper fascia take a lot of time to make a die, so it is necessary to determine the part shape quickly to shorten the term. Therefore, performance verification by simulation is important. However, due to issues such as material property and complicated part shapes, reproduction of phenomena such as deformation and failure are sometimes not sufficiently accurate in simulations of plastic parts. Creating a die, testing part, and evaluating its performance in such a situation may raise the possibility of inadequate performance. In that case, it is necessary to modify the die, which requires extra cost and time. Therefore, high simulation accuracy is necessary to avoid such risks.
Various sensors have been equipped in cars recently from the viewpoint of accident prevention. Among them, a parking brake sensor that needs to be managed properly the mounting angle is equipped on the rear bumper fascia. The deformation behavior of plastic components such as a bumper fascia is increasingly investigated in low-speed crash load cases. By evaluating the deformation of the bumper fascia and the angle change of the sensor in low-speed crash load cases, a suitable location to place the sensor in a place where the angle change is small, or optimization of the thickness and the shape of the bumper fascia can be investigated in advance. It is important to enhance simulation accuracy of plastic parts in order to think about performance in parallel with car design.
In the low speed crash load case, the part deforms up to a maximum indentation (loading phase) and then rebounds (the unloading phase). The commonly used elastic-viscoplastic material models (***MAT_024**) can describe the observed deformations in the loading phase, but it underestimates the deformations in the unloading phase.
The accurate depiction of this behavior can be used to further optimize these components. In this project several LS-DYNA® material models were investigated for their accurate, stable and numerically efficient depiction of dynamic unloading cases of plastic parts. Then a material model was selected to further investigate its capability in low-velocity rear impact analysis of a full-vehicle model.

2 Material models

The possibility of modelling the unloading behavior using existing models in LS-DYNA® was investigated as an initial pre-study. A test program was defined for a thermoplastic material (PP) at the coupon level and tests were conducted with the IMPETUS® system (dynamic) and with a universal testing machine for the static cases at room temperature. The samples for the tests were obtained from injection molded plates [1] with 2-millimeter thickness. These tests comprise of static and dynamic 3-point-bending, static and dynamic tensile as well as static and dynamic puncture. With the experimental results in hand, different material models were investigated to determine their suitability in modelling the unloading behavior. For the FE-models, shell elements (**ELFORM**=16) were used with 2-millimeter size and with 5 integration points over the thickness.

2.1 Pre-study – possibility of modelling unloading behavior

As a starting point, a ***MAT_024** material card was generated by reverse engineering with VALIMAT® and LS-Opt® to describe the material behavior [2]. The Young's Modulus was optimized to the dynamic bending tests. The hardening curves and the strain rate dependency were parametrized and fitted to the 3-point bending load cases at different velocities. This approach has the drawback that other load cases like the tensile test and the puncture test as well as the unloading/rebound behavior cannot be depicted by the model. This material model was modified through the addition of viscoelasticity using

the ***MAT_ADD_INELASTICITY** option. The addition of the viscoelasticity part at the start did not change the response in the unloading phase.

The ***MAT_101** material model was considered next. Unloading behavior can be defined directly in the material model. Stability issues were encountered while dealing with complex load cases at the component level. Although it is a promising option to model the unloading, more investigation needs to be done to find the underlying cause with regards to stability in the simulation model as well as the material subroutine.

A hyperelastic material model ***MAT_083** was also investigated in combination with ***MAT_ADD_INELASTICITY** for the definition of plasticity. Parameter fitting was cumbersome with this material model for the thermoplastic material especially in the unloading phase (SHAPE and HU parameters) and stability issues were encountered. This approach was abandoned and not followed further.

The ***MAT_SAMP_Light(*MAT187L)** provides an interesting option to model the tension-compression asymmetry and viscoelasticity. This leads to good agreement in the force displacement curves in all the load cases. However, the unloading behavior could not be captured with this material model.

The ***MAT_SAMP-1 (*MAT187)** model was investigated in the next step [3]. Instead of an unloading modulus, an elastic damage curve can be defined to depict the unloading behavior. Viscoelastic material behavior can also be added to the material model with the **LCEMOD** option. A ***MAT_SAMP-1** material model was then calibrated based on the 3-point bending and the tensile tests using the Drucker-Prager formulation. The static and dynamic bending modulus served as the lower and upper limits for the definition of viscoelasticity as a function of the strain rate. A simple parabolic damage progression with a maximum damage plateau was defined for the elastic damage curve with VALIMAT® (see Equation 1). Here, d_{cap} is the maximum damage, and d_{eps} represents the equivalent plastic strain to reach this damage cap.

$$D(\varepsilon_p) = -\frac{d_{cap}}{{d_{eps}}^2} \cdot \left(min(\varepsilon_p, d_{eps})\right)^2 + \left(2 \cdot \frac{d_{cap}}{d_{eps}}\right) \cdot min(\varepsilon_p, d_{eps}) \quad (1)$$

The hardening curves of the previous fit were adjusted (see Equation 2 & 3). The yield stress values for tension $\sigma_{y,LCID\_T}$ and compression $\sigma_{y,LCID\_C}$ were compensated for the additional damage curve LCID-D with the curve values $D(\varepsilon_p)$ and the originally fitted hardening curves for tension $LCID\_T_{old}(\varepsilon_p, \dot{\varepsilon}_p)$ and compression $LCID\_C_{old}(\varepsilon_p, \dot{\varepsilon}_p)$.

$$\sigma_{y,LCID\_T}(\varepsilon_p, \dot{\varepsilon}_p) = \left(LCID\_T_{old}(\varepsilon_p, \dot{\varepsilon}_p)\right) / \left(1 - D(\varepsilon_p)\right) \quad (2)$$

$$\sigma_{y,LCID\_C}(\varepsilon_p, \dot{\varepsilon}_p) = \left(LCID\_C_{old}(\varepsilon_p, \dot{\varepsilon}_p)\right) / \left(1 - D(\varepsilon_p)\right) \quad (3)$$

This model was then fitted to the low-speed dynamic bending test with observed rebound.
The investigations at the coupon level showed that the ***MAT_101** and ***MAT_SAMP-1** with viscoelasticity and damage were the two best options to model the unloading behavior of the material. In terms of computational times, the ***MAT_101** showed similar performance to the ***MAT_024** as depicted in Fig 1. The ***MAT_SAMP-1** with viscoelasticity and elastic damage was almost 7x slower than the ***MAT_024** but also the most stable and accurate at the coupon level.

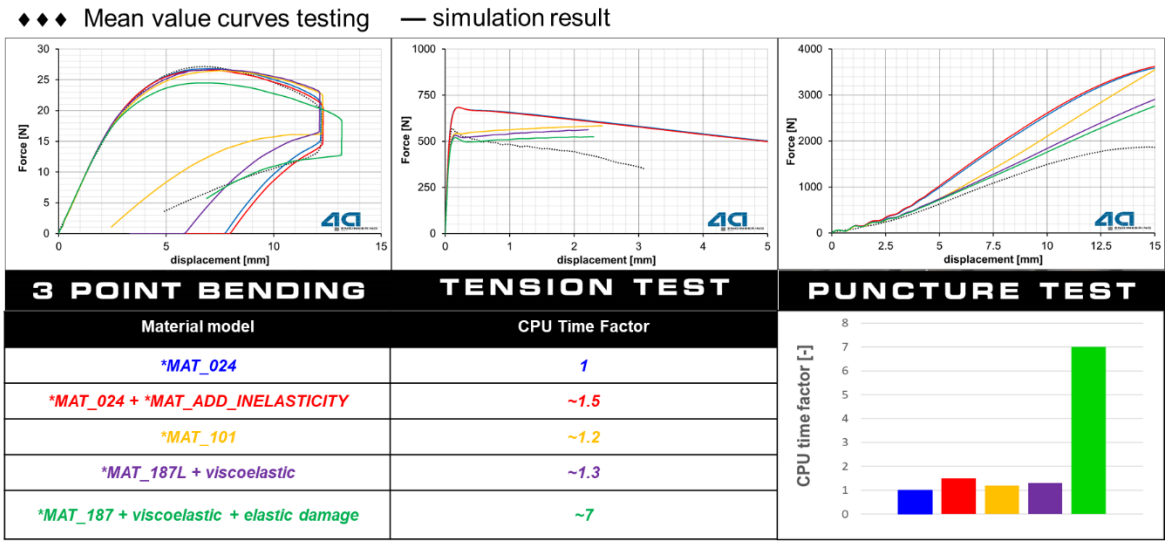

Material model	CPU Time Factor
*MAT_024	1
*MAT_024 + *MAT_ADD_INELASTICITY	~1.5
*MAT_101	~1.2
*MAT_187L + viscoelastic	~1.3
*MAT_187 + viscoelastic + elastic damage	~7

Fig.1: Summary of the different material model behavior and their computational times in relation to ****MAT_024*** *for dynamic bending, dynamic tension and dynamic puncture test for the PP material.*

2.2 *MAT_SAMP-1 with viscoelasticity and elastic damage

The ***MAT_SAMP-1** material model was then further optimized to obtain a good correlation to the individual test cases as depicted in Figure 2. The damage curve parameters were fit to the 0.6 m/s 3-point bending load case. This case was deemed most representative for the use in low speed crash simulations. Additionally, the internal failure model, which handles element deletion, of ***MAT_SAMP-1** was fitted to the tensile and the puncture test results. **EPFAIL** was defined negatively to add some strain rate dependency for the equivalent plastic failure strain as observed in the static and dynamic tensile tests. A LCID_TRI curve was also defined to scale the failure strain up in case of a compression load to prevent element deletion and to reduce the failure strain to capture the puncture test failure. A short constant equivalent plastic strain increment was added with **DEPRPT**.

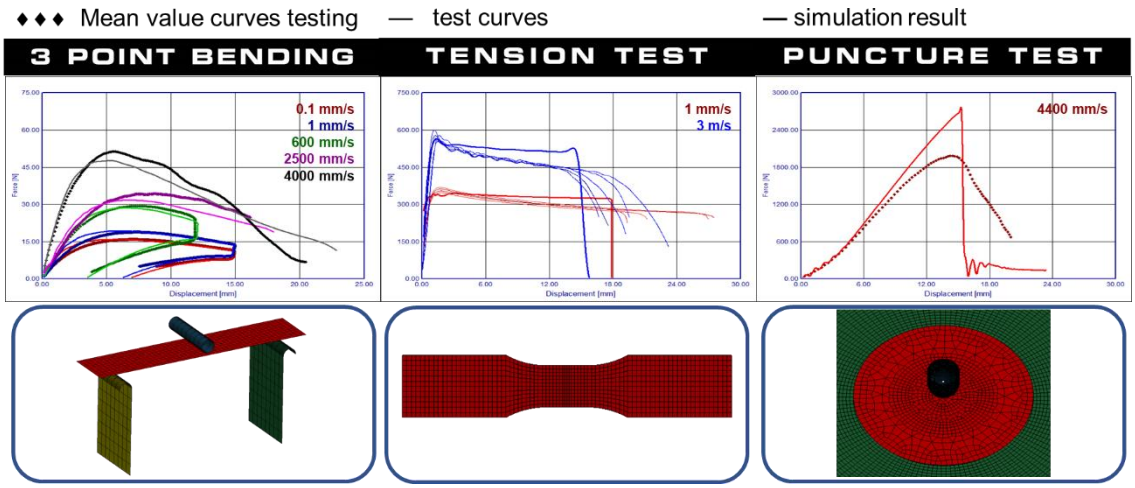

Fig.2: Final ****MAT_SAMP-1*** *with viscoelasticity and elastic damage – results for different static and dynamic load cases and a depiction of the FEM model.*

The end displacement of the 3-point bending specimen (~ 3 mm) is greatly overestimated by using the standard ***MAT_024** material model (~8 mm). The calibrated ***MAT_187** material model with viscoelasticity and damage can depict this recovery on the coupon level (see Figure 3).

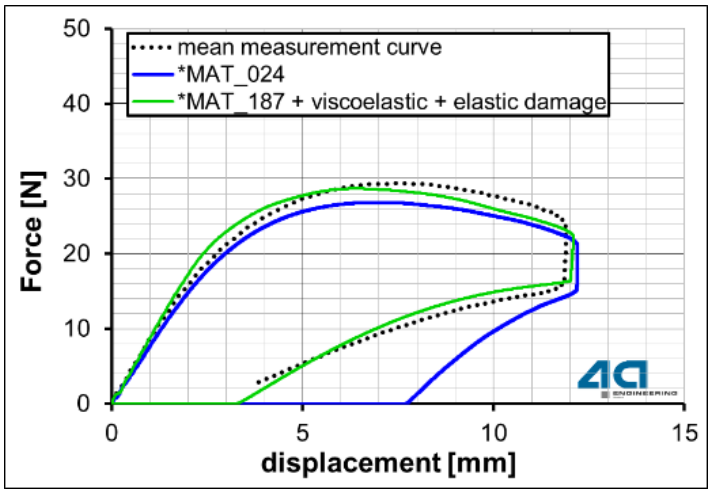

*Fig.3: Comparison of observed Force displacement curves of the dynamic 3-point bending test at 0.6 m/s to the standard ***MAT_024** and the fully calibrated ***MAT_187** material models with viscoelasticity and damage.*

3 Full vehicle simulation – bumper deformation during unloading

The material model examined in chapter 2.2 was applied to the full vehicle simulation to verify the reproducibility of the test. The test compared with the simulation was a low-speed crash test called ECE42. It is the test in which a barrier impacts a car at 2.5mph in the horizontal direction to evaluate damages applied to parts in rear portion of the car (Fig.4-1). There are two ways to strike the barrier,

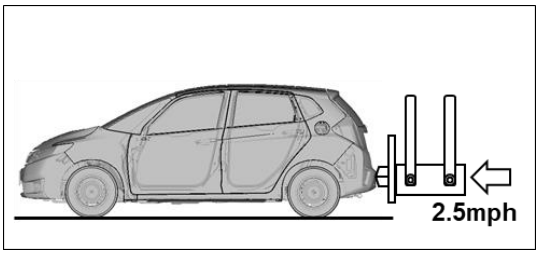

Fig.4-1: Overview of ECE42

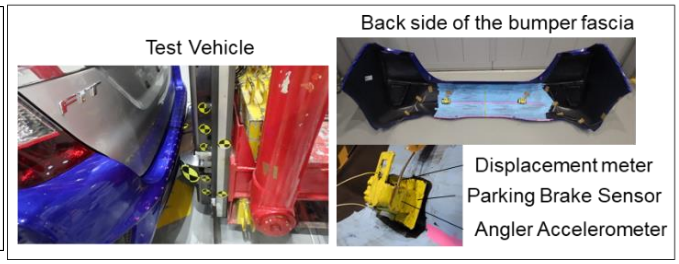

Fig.4-2: Overview of the measurement

and the simulation was verified by a longitudinal impact test. The items measured in the vehicle test were the amount of deformation and the angle change of the parking brake sensor equipped on the rear bumper fascia. There were two parking sensors equipped on the rear bumper fascia, and displacement meters and angular accelerometers are attached to each sensor (Fig.4-2). The test was recorded with a high-speed camera to track the deformation of the bumper fascia during the impact.
First, the deformation observed in the test and the simulation are compared in Fig.5. It shows the deformation at 0msec before impact, 195msec at the maximum deformation and 500msec at the end of

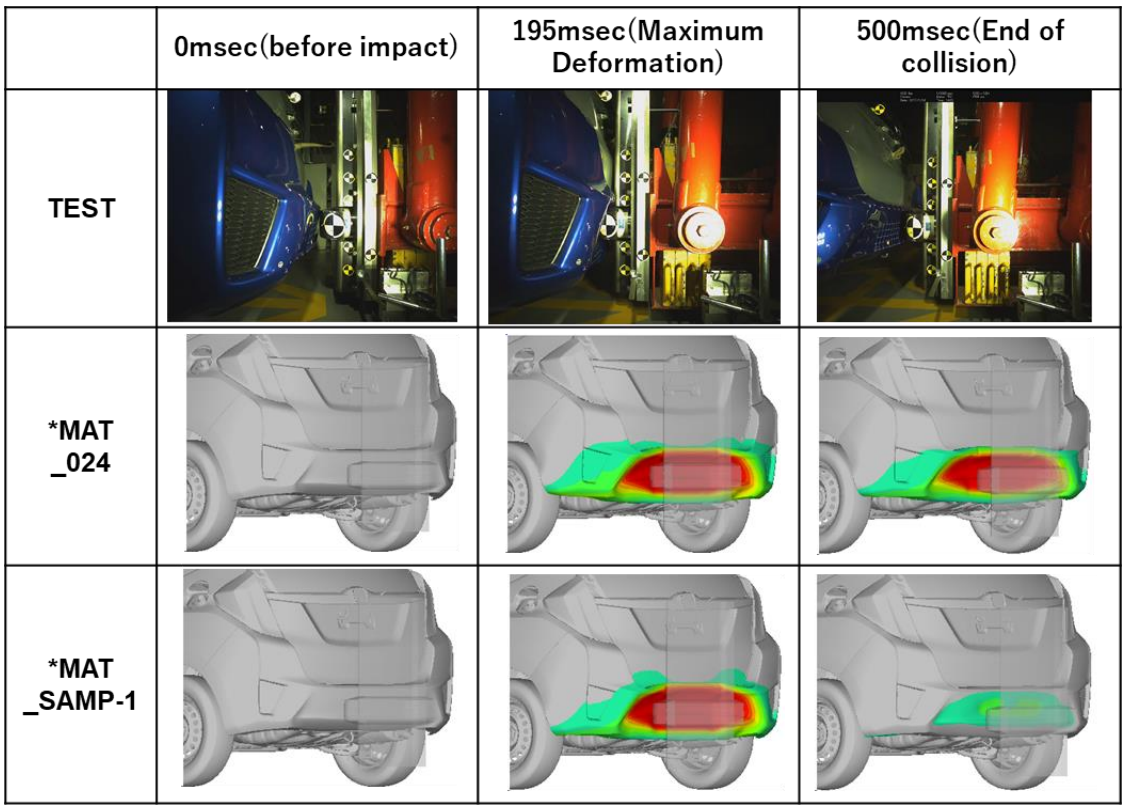

*Fig.5: Comparison the deformation in x-direction of the Test, ***MAT_024** and ***MAT_SAMP-1** with viscoelasticity and elastic damage*

impact. The contour represents the magnitude of the displacement in the X-axis direction (front to back direction of the car). The deformation of the test was almost restored, but ***MAT_024** was not completely restored and the reproducibility of the test was low. On the other hand, ***MAT_SAMP-1** showed the result closer to the test, with the deformation almost restored. Fig.6-1 is a graph of time-deformation curve of the left side sensor. The black line shows the actual vehicle test, the blue line shows the calculation result of ***MAT_024**, and the red line shows ***MAT_SAMP-1** with viscoelasticity and elastic damage. ***MAT_024** showed a difference of 6% to the test at 200msec where the maximum deformation occurred,

while ***MAT_SAMP-1** showed 10% difference. They both showed deformation characteristics similar to the test up to 285 msec. After that, the deformation of ***MAT_024** stopped and maintained the same value, while ***MAT_SAMP-1** decreases faster with vibration than the test and returns to the state before the collision as in the test. Fig.6-2 is a graph of time-angle change curve of the left side sensor. The maximum angle change in the vehicle test was 25 degrees, ***MAT_024** was 15 degrees, and ***MAT_SAMP-1** was 21 degrees, around 100 msec. ***MAT_024** maintained 15 degrees after 285msec and did not return to the state before the collision similar to the deformation. ***MAT_SAMP-1** showed similar characteristics to the test after 100 msec. Although the angle change decreased faster than the test, the remaining angle change was 2 degrees, at the end of the collision, which was the same as the test. Fig.7 is a comparison of the full vehicle calculation time. There was a 7 times difference in calculation time at the component level, but it was 15% difference between *MAT_024 and *MAT_SAMP-1 in the full-car analysis because

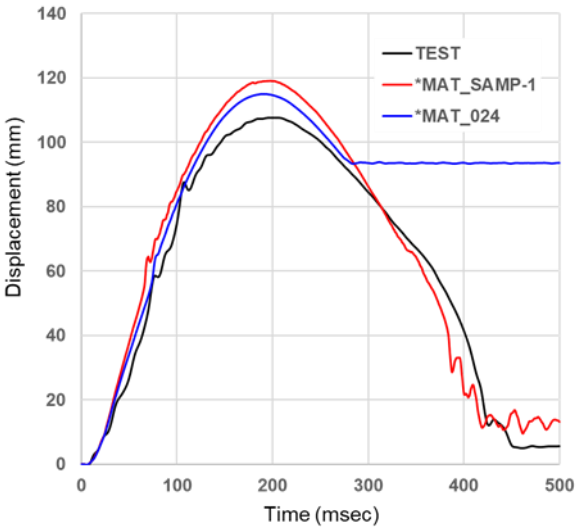

Fig. 6-1: Displacement of the Bumper Fascia

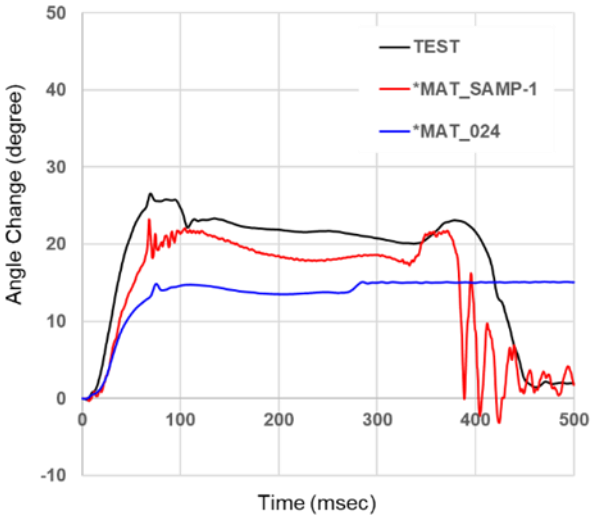

Fig. 6-2: Angle Change of the Sensor

the material was only changed in the rear bumper fascia.

It was confirmed that ***MAT_SAMP-1** can reproduce the deformation and sensor angle change after the unloading process of the collision.

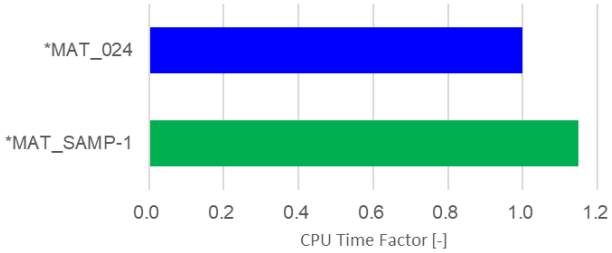

Fig. 7: Comparison of the calculation time

4 Summary

Different material models were investigated for their suitability to model the bumper return deformation (unloading) for an unreinforced plastic material. The material was tested under different static and dynamic load cases to generate experimental data with the IMPETUS® test system in combination with a universal testing machine. This data was then used further for an initial pre-study of the material models. Out of the different material models, the ***MAT_SAMP-1** model with viscoelasticity and elastic damage was then further optimized with VALIMAT® to obtain a suitable material model that depicts this unloading behavior.

This generated material model was used in a full vehicle simulation (ECE42) in a low speed crash case. The comparison between the industry standard ***MAT_024** and the ***MAT_SAMP-1** model shows very clearly that the unloading behavior is well represented.

5 Literature

[1] 4a test packages, https://www.4a-engineering.at/downloads/testpackages.pdf

[2] Reithofer. P et.al, Material Models For Thermoplastics In LS-DYNA® - From Deformation To Failure, 15th International LS-DYNA Users conference, 2018

[3] Kolling. S et.al, SAMP-1: A Semi-Analytical Model for the Simulation of Polymers, 4th LS-DYNA Anwenderforum, 2005.

[4] LS-DYNA® Keywords User's Manual – Volume I ,https://www.dynasupport.com/manuals/ls-dyna-manuals/ls-dyna_manual_volume_i_r12.pdf

[5] LS-DYNA® Keywords User's Manual – Volume II, https://www.dynasupport.com/manuals/ls-dyna-manuals/ls-dyna_manual_volume_ii_r12.pdf